frontiers | Frontiers in Materials

TYPE Original Research
PUBLISHED 08 March 2023
DOI 10.3389/fmats.2023.1162270

OPEN ACCESS

EDITED BY
Jiantie Xu,
South China University of Technology, China

REVIEWED BY
Jian Xie,
Hanshan Normal University, China
Yuyang Hou,
Commonwealth Scientific and Industrial Research Organisation (CSIRO), Australia

*CORRESPONDENCE
Chen Zhao,
czhao@gdut.edu.cn
Xiaoxian Zhang,
15002007401@163.com
Yonggang Min,
ygmin@gdut.edu.cn
Kewei Shu,
shukw@sust.edu.cn

SPECIALTY SECTION
This article was submitted to Energy Materials, a section of the journal Frontiers in Materials

RECEIVED 09 February 2023
ACCEPTED 27 February 2023
PUBLISHED 08 March 2023

CITATION
Yuan W, Zhao C, Zhang X, Min Y and Shu K (2023), Facile fabrication of flexible and adhesive micro-supercapacitor tapes from conducting polymer solution for self-powered wearable sensing system. *Front. Mater.* 10:1162270. doi: 10.3389/fmats.2023.1162270

Facile fabrication of flexible and adhesive micro-supercapacitor tapes from conducting polymer solution for self-powered wearable sensing system

Wenxiong Yuan[1], Chen Zhao[1]*, Xiaoxian Zhang[2]*, Yonggang Min[1]* and Kewei Shu[3]*

[1]School of Materials and Energy, Guangdong University of Technology, Guangzhou, China, [2]Pulmonary and Critical Care Medicine, Guangzhou Institute of Respiratory Health, National Clinical Research Center for Respiratory Disease, National Center for Respiratory Medicine, State Key Laboratory of Respiratory Diseases, The First Affiliated Hospital of Guangzhou Medical University, Guangzhou, China, [3]Xi'an Key Laboratory of Advanced Performance Materials and Polymers, Shaanxi Key Laboratory of Chemical Additives for Industry, Shaanxi University of Science and Technology, Xi'an, China

Flexible micro-supercapacitor (MSC) with in-plane electrodes has attracted significant attention as microscale energy storage device. Especially, flexible MSCs with adhesion properties are of great interest for wearable electronics. Here, we demonstrate a facile and cost-effective mask-assisted drop-casting method to fabricate adhesive MSC on medical tape using dimethyl sulfoxide (DMSO) doped poly (3,4-ethylenedioxythiophene):poly (styrenesulfonate) (PEDOT:PSS) aqueous solution. The fabricated MSC with poly (vinyl alcohol)/H_3PO_4 gel electrolyte exhibits an areal specific capacitance of 10.96 mF cm^{-2} at a current density of 0.1 mA cm^{-2} with excellent mechanical flexibility. The MSC can be attached on various substrates due to the stickiness of the medical tape. For practical application, the MSC can be coupled with a solar cell to achieve a stand-alone power supply system for a flex senor in monitoring finger movements. Therefore, we believe that the mask-assisted drop-casting method paves a new way to develop flexible and adhesive MSCs for self-powered integrated wearable electronics.

KEYWORDS

wearable, PEDOT:PSS, micro-supercapacitor, strain sensor, self-powered

1 Introduction

The rapid progress in miniaturized and wearable electronics has significantly triggered the demand for flexible and microscale energy storage devices such as micro-batteries and micro-supercapacitors (MSCs) (Zheng et al., 2019). Especially, flexible MSCs with in-plane electrodes are of great interest for powering wearable electronics due to the merits of high power density, long operating lifetime, high safety, and excellent conformability (Zhao et al., 2018). The in-plane electrode geometry is free of separator and can facilitate the diffusion of electrolyte ions to improve the electrochemical performance (Chen et al., 2018). Furthermore, the flexible MSCs can be easily integrated with energy conversion units such as solar cells and nanogenerators on one substrate as stand-alone power supply systems to drive various functional devices (Lin et al., 2019; Zhang et al., 2021).

To date, tremendous effects have been made to develop various patterning techniques for fabricating flexible MSCs. The patterning of in-plane electrodes with different types of active materials can be classified into two categories: bottom-up and top-down (Zhao et al., 2020). In the bottom-up approach, the current collectors are fabricated onto a flexible substrate followed by the deposition of active materials through diverse approaches such as electrodeposition (Wang et al., 2011), electrophoretic deposition (Liu et al., 2013), spray coating (Kim et al., 2015), mechanical pressing (Gao et al., 2018), and printing (Wang et al., 2014). While in the top-down strategy, an etching process is applied to a thin film of active materials to remove unwanted parts achieving interdigitated electrodes. Various etching methods have been involved including dry etching (Wu et al., 2015; Liu et al., 2016; Salles et al., 2018) and wet etching (Xue et al., 2011). The flexible substrates are commonly polymer foil (Lin et al., 2019), paper (Kurra et al., 2016), and textile/fabric (Pu et al., 2016), which could sustain different mechanical deformations, such as bending, folding, stretching and compressing. However, few of those substrates could be directly mounted onto the human skin or garments because they are generally non-adhesive. The introducing of adhesive substrates may facilitate the attachment of flexible MSCs on various targets to exert the function. Zhu et al. (2019) reported skin-mountable plaster-like MSCs using adhesive medical tapes. Conductive graphite layers were coated on the medical tape by a drawing process and then MnO_2 was deposited onto the graphite layers by a mild *in situ* redox reaction serving as active material. The fabricated MSCs not only showed superior adhesion, good flexibility and biocompatibility, but also possessed outstanding electrochemical performances. However, simple and high throughout electrode patterning methods are still under exploration for high efficient fabrication of adhesive MSCs for wearable electronics.

Herein, we report a facile approach to fabricate adhesive MSCs using aqueous conducting polymer ink and its integration with indoor solar cell for self-powered wearable sensing system. A mask-assisted drop-casting method was proposed to prepare the planar electrodes on 3M medical tape using conducting polymer poly (3,4-ethylenedioxythiophene):poly (styrenesulfonate) (PEDOT:PSS) aqueous solution. PEDOT:PSS was doped with dimethyl sulfoxide (DMSO) to enhance the conductivity, serving as both current collector and active material. The fabricated MSC with polymer electrolyte poly (vinyl alcohol)/H_3PO_4 (PVA/H_3PO_4) showed an areal specific capacitance of 10.96 mF cm^{-2} at a current density of 0.1 mA cm^{-2}. The tape-like MSCs can be attached on various targets. The flexible MSC made by this simple approach would be used in a self-powered energy supple system for flex sensor in recording finger movements, showing its great promise as energy storage devices for wearable electronics and Internet of Things.

2 Materials and methods

Fabrication of the MSC: PEDOT:PSS (PH1000, Heraeus) was mixed with 5wt% of DMSO (Aladdin Bio-Chem) for 12 h under magnetic stirring, then it was drop-casted onto a piece of medical tape (2733-50, 3M) that was covered by a stainless steel mask with a designed parallel electrode shape and dried at 60°C for 1 h. PVA/H_3PO_4 gel electrolyte was prepared following our previous report (Zhao et al., 2013), and the gel electrolyte solution was drop-casted onto the localized electrode area and dried at 40°C for 12 h for solidification to get the solid-state MSC.

Assembly of the integrated sensing system: The commercialized solar cell and flex sensor purchased from the online shop (www.taobao.com) were used as the energy-harvesting unit and sensing unit, respectively. The solar cell and the MSC were connected in parallel to achieve a stand-alone power supply system, while the MSC, a 47 kΩ resistor, and the flex sensor were connected in series. The resistor was used to adjust the current in the circuit.

Characterizations: The surface morphology and microstructure of the samples were characterized using a field emission scanning electron microscope (FE-SEM, SU8010, Hitachi). A microscope (BA310Me, Motic) was used to observe the patterned PEDOT:PSS electrodes. Raman spectra of the PEDOT:PSS samples were obtained using a Raman spectrometer (LabRAM HR Evolution, HORIBA Jobin Yvon) with a 532 nm diode laser.

Measurements: The current-voltage *(I-V)* curves of the electrodes, cyclic voltammetry (CV), galvanostatic charge–discharge (GCD), and electrochemical impedance spectroscopy (EIS) tests of the MSC were performed on an electrochemical workstation (CHI 760E, Chenhua Instruments). EIS was measured at the open circuit potential in the frequency range from 100 kHz to 0.01 Hz with potential amplitude of 5 mV. Cycling stability test and self-discharge test of the MSC were conducted on a battery test system (CT-4008-5V10mA, Neware Electronics). Bending tests of the MSC were conducted on a manual linear stage (DSM 100S-65140L, Zolix). Photo charging test of the MSC, resistance changes of the flex senor, and the current signal of the integrated flex sensor were measured using a digital multimeter (34465A, Keysight).

3 Results and discussion

Figure 1 illustrates the fabrication process of an individual MSC with a pair of parallel electrodes on medical tape by the mask-assisted drop-casting method. The DMSO doped PEDOT:PSS aqueous solution was drop-casted onto a piece of medical tape that was covered by a mask with a designed parallel electrode shape. In this work, a rectangular shape with the length of 15 mm and width of 1.0 mm was chosen to imitate a single electrode. After drying at 60°C for 1 h, a polymer gel electrolyte of poly (vinyl alcohol)/H_3PO_4 (PVA/H_3PO_4) was drop-casted onto the localized electrode area and dried at 40°C for 12 h to finalize the fabrication of the tape-like solid-state MSC.

Wetting and absorption of the DMSO doped PEDOT:PSS aqueous solution is limited on the medical tape due to its low hygroscopicity. The droplet of DMSO doped PEDOT:PSS aqueous solution did not wet the medical tape immediately, and a circular PEDOT:PSS pattern with sharp edges and a smaller area than that of the initial droplet was obtained after drying (Figure 2A). As a result, it is possible to make various patterns on the medical tape using a pre-designed mask with DMSO doped PEDOT:PSS aqueous solution. Heart-shaped and circular patterns nearly identical to the masks were successfully achieved (Figures 2B–E). This method is also applicable to other aqueous solutions, such as

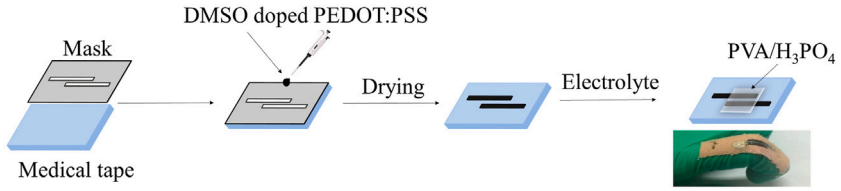

FIGURE 1
Schematic illustration of the fabrication process of the adhesive MSC.

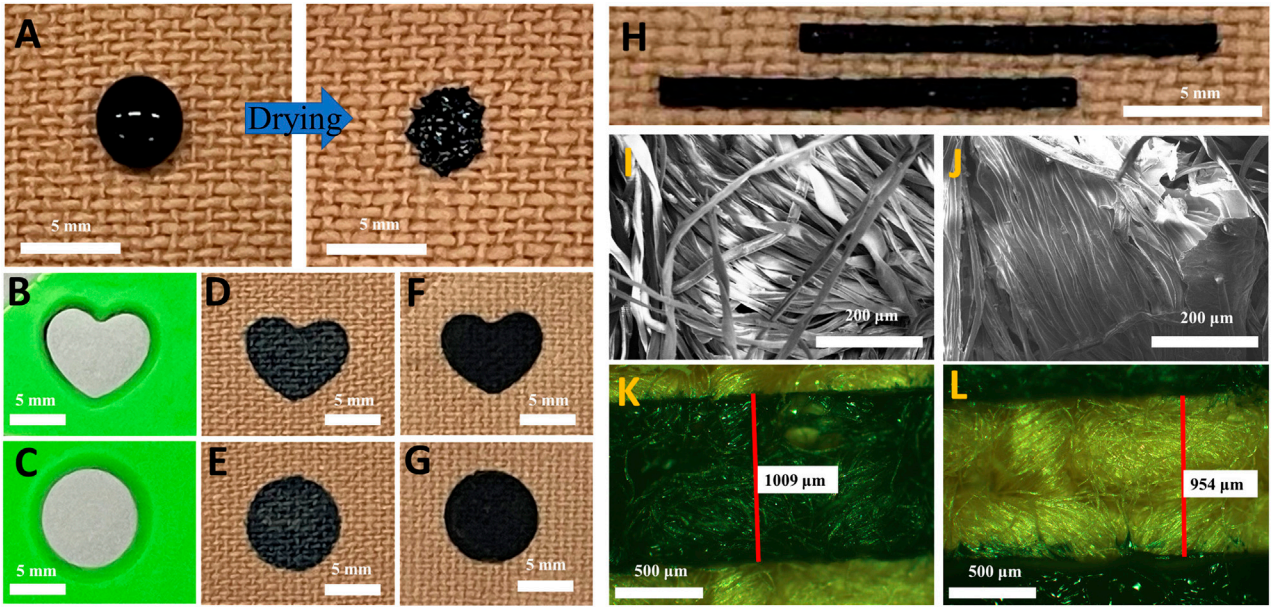

FIGURE 2
Patterning the planar electrodes on the medical tape. Photos: **(A)** the DMSO doped PEDOT:PSS droplet before and after drying on the medical tape. **(B)** Heart-shaped mask. **(C)** Circular mask. **(D, E)** Heart-shaped and circular PEDOT:PSS patterns on medical tape. **(F, G)** Heart-shaped and circular MXene patterns on medical tape. **(H)** A pair of planar PEDOT:PSS electrodes on medical tape. SEM images of the medical tape **(I)** before and **(J)** after PEDOT:PSS coating. Optical images showing **(K)** width of the PEDOT:PSS electrode and **(L)** the interspace between two electrodes.

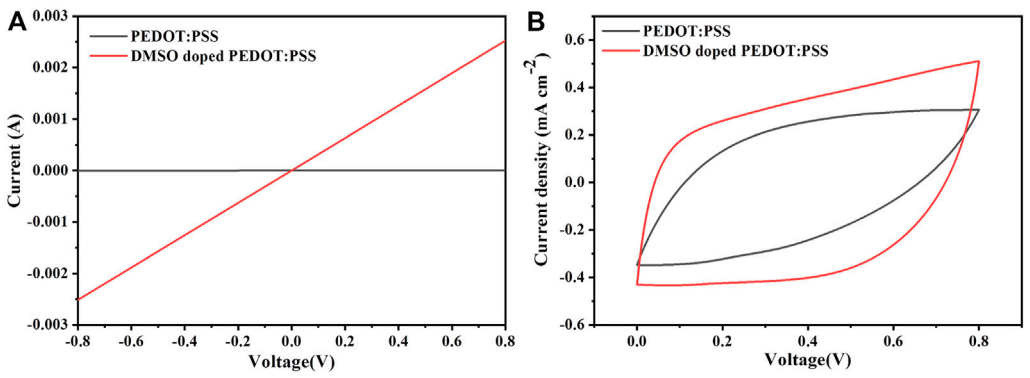

FIGURE 3
(A) I-V curves of the electrodes prepared with pure PEDOT:PSS and DMSO doped PEDOT:PSS. **(B)** CV curves (at 100 mV s^{-1}) of the MSCs with electrodes prepared with pure PEDOT:PSS and DMSO doped PEDOT:PSS.

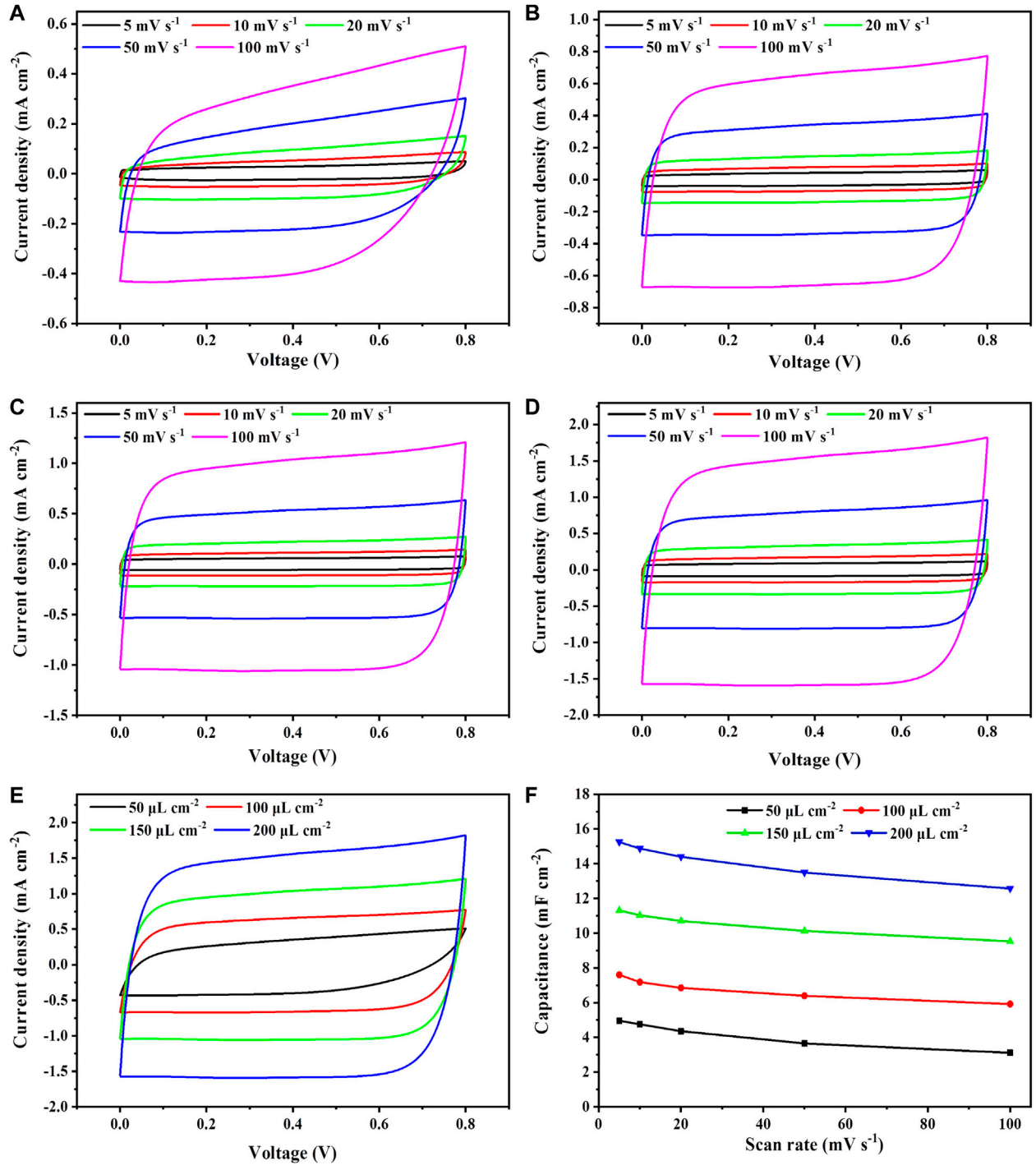

FIGURE 4
CV curves of the MSCs with different DMSO doped PEDOT:PSS solution loadings on the electrodes: **(A)** 50 μL cm^{-2}, **(B)** 100 μL cm^{-2}, **(C)** 150 μL cm^{-2}, and **(D)** 200 μL cm^{-2}. **(E)** Comparison of the CV curves of the MSCs at 100 mV s^{-1}. **(F)** Areal specific capacitances of the MSCs calculated from CV curves.

MXene solution (Figures 2F, G), showing its universality. Figure 2H shows a pair of parallel PEDOT:PSS electrodes on the medical tape. A thin layer of PEDOT:PSS could be clearly observed (Figures 2I, J). The thickness of the electrode increased from 68 to 180 μm as the loading of PEDOT:PSS increased from 50 to 200 μL cm^{-2} (Supplementary Figure S1). The patterned electrodes were imaged using an optical microscopy. Typical width of a single electrode was measured to be around 1,000 μm (Figure 2K). A straight gap of about 950 μm wide was found between two electrodes (Figure 2L).

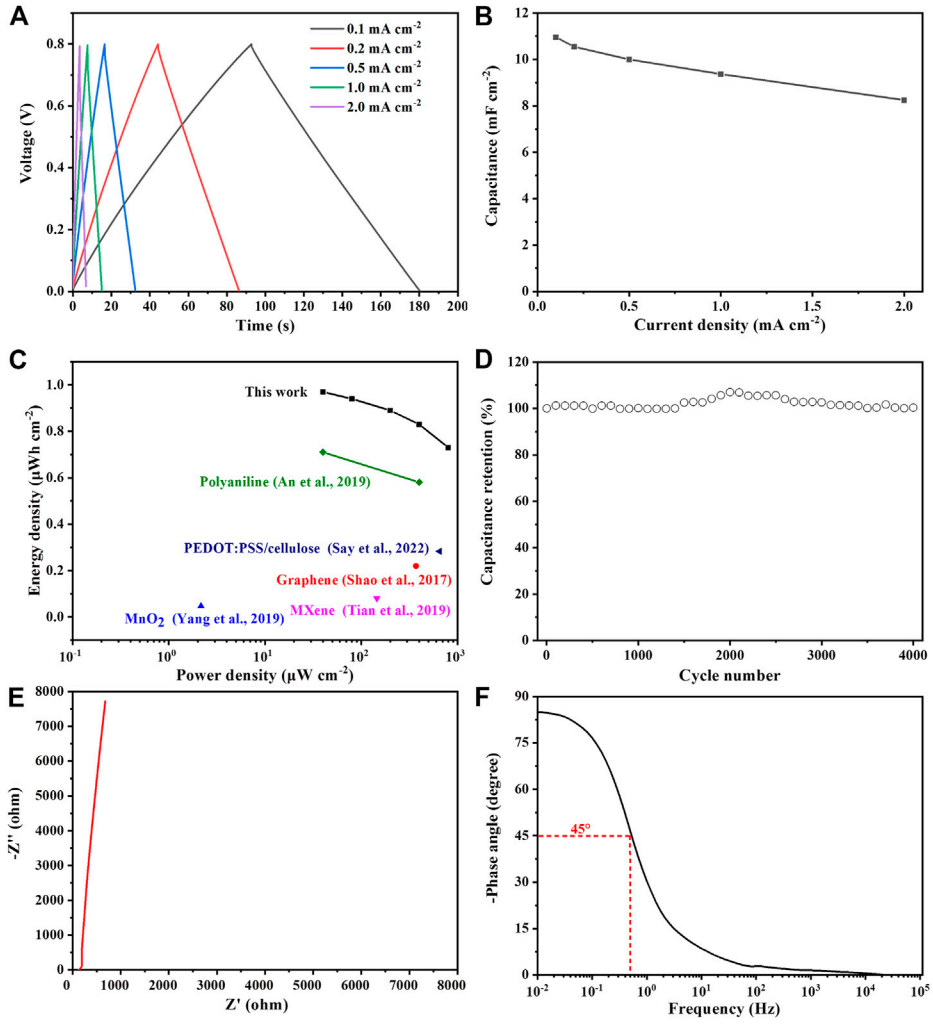

FIGURE 5
Electrochemical performance of the MSC-150. **(A)** GCD curves and **(B)** areal specific capacitances at different current densities. **(C)** Comparison of energy and power density with that of previously reported flexible MSCs. **(D)** Cycling performance at 1 mA cm^{-2} for 4,000 cycles. **(E)** Nyquist plot. **(F)** Bode plot.

I-V curves of the electrodes were recorded to investigate the electrical properties. At the same loading (50 μL cm^{-2}), the electrode prepared with DMSO doped PEDOT:PSS showed higher conductivity than that prepared with pure PEDOT:PSS, as evidenced by the increased slope shown in the *I-V* curves (Figure 3A). The effect of DMSO was further confirmed by Raman Spectroscopy (Supplementary Figure S2). The peak between 1,400 and 1,500 cm^{-1} corresponding to the $C_\alpha = C_\beta$ stretching vibration of the thiophene ring on the PEDOT chains, shifted to red after the addition of DMSO, indicating the changes of the PEDOT chain from a benzoid to a quinoid structure. And spontaneously the PEDOT chains changed from coil to expanded-coil or linear conformations, leading to enhanced conductivity (Ouyang et al., 2004). The electrical properties of the electrodes were further investigated in terms of the material loadings. The resistance of the electrode gradually decreased due to the more efficient conducting network formed with higher material loading (Supplementary Figure S3). Compared to the MSC with pure PEDOT:PSS electrodes, the device with DMSO doped PEDOT:PSS electrodes showed better electrochemical performance due to the increased conductivity (Figure 3B) (Manjakkal et al., 2020). Hence only the electrochemical performance of the MSC based on DMSO doped PEDOT:PSS was studied.

The tape-like flexible MSC was assembled with two symmetric rectangular-shaped electrodes with total active geometrical area of 0.2 cm^2, while a thin layer of PVA/H_3PO_4 was employed as gel electrolyte. The electrochemical properties of the flexible MSC were initially evaluated by CV tests in the voltage window of 0–0.8 V. The CV curves of the MSCs with different material loadings are shown in Figures 4A–D. When the loadings of DMSO doped PEDOT:PSS solution on the

electrodes were varied at 50, 100, 150 and 200 μL cm^{-2}, the corresponding MSC devices (denoted as MSC-50, MSC-100, MSC-150 and MSC-200) showed nearly rectangular CV curves at different scan rates ranging from 5 to 100 mV s^{-1}, indicative of ideal capacitive behaviors. And the capacitance increased with growing amount of DMSO doped PEDOT:PSS solution (Figure 4E). The areal specific capacitances calculated based on CV curves are plotted in Figure 4F. The MSC-50 exhibited an areal specific capacitance of 4.96 mF cm^{-2} at the scan rate of 5 mV s^{-1} with capacitance retention of 62.7% (3.11 mF cm^{-2}) as the scan rate reached 100 mV s^{-1}. Further increasing the loading to 100 and 150 μL cm^{-2} significantly improved the areal specific capacitance at 5 mV s^{-1} (7.60 and 11.31 mF cm^{-2}, respectively) with enhanced capacitance retention at 100 mV s^{-1} (77.9% and 84.3%, respectively). The improved rate capability can be attributed to the more efficient conducting network formed with higher PEDOT:PSS loading. Continuously increasing the loading (200 μL cm^{-2}) resulted in further improvement in capacitance (15.25 mF cm^{-2} at 5 mV s^{-1}), however, deteriorated capacitance retention (82.4%) was obtained due to the limited ion diffusions in the thickened electrodes. Thus, in the following tests, the loading of DMSO doped PEDOT:PSS solution was chosen to be 150 μL cm^{-2} (MSC-150) when taking the reasonably high capacitance and rate capability into account.

The MSC-150 was then galvanostatically charged/discharged at current densities ranging from 0.1 to 2 mA cm^{-2}. Regardless of the current densities, all the curves showed near-ideal symmetrical triangular shapes (Figure 5A), indicating the fast kinetics. The areal specific capacitances at different current densities calculated based on the curves are summarized in Figure 5B. The MSC-150 exhibited an areal specific capacitance of 10.96 mF cm^{-2} at the current density of 0.1 mA cm^{-2}. The areal specific capacitance of our approach is higher than that of MSCs fabricated with carbonaceous materials, such as reduced graphene oxide (8.19 mF cm^{-2}) (Pu et al., 2016), Nitrogen-doped reduced graphene oxide (3.4 mF cm^{-2}) (Liu et al., 2014), and graphene/multiwalled carbon nanotubes (2.54 mF cm^{-2}) (Yun et al., 2014). And it is also comparable to that of MSCs with pseudocapacitive materials, such as MnO_2 (11.9 mF cm^{-2}) (Hu et al., 2016), polyaniline (11.76 mF cm^{-2}) (An et al., 2019), polypyrrole (8.15 mF cm^{-2}) (Zhu et al., 2017), and PEDOT:PSS/cellulose (3.18 mF cm^{-2}) (Say et al., 2022). As the current density increased to 2.0 mA cm^{-2}, the areal specific capacitance remained at 8.25 mF cm^{-2}. More than 75% capacitance was retained while the current density increased by 20-folds, showing good rate performance.

Energy density and power density are two crucial parameters of MSCs for practical applications. As shown in the Ragone plot (Figure 5C), the areal energy density of the MSC-150 achieved 0.97 μWh cm^{-2} at a power density of 40 μW cm^{-2}, and retained at 0.73 μWh cm^{-2} at a power density of 800 μW cm^{-2}. Such performance is superior or comparable to that of the reported MSCs assemble with different active materials, such as graphene (0.22 μWh cm^{-2} at 0.37 mW cm^{-2}) (Shao et al., 2017), MnO_2 (0.047 μWh cm^{-2} at 2.16 μW cm^{-2}) (Yang et al., 2019), MXene (0.08 μWh cm^{-2} at 145 μW cm^{-2}) (Tian et al., 2019), polyaniline (0.71 μWh cm^{-2} at 40 μW cm^{-2}) (An et al., 2019), and PEDOT:PSS/cellulose (0.283 μWh cm^{-2} at 0.65 mW cm^{-2}) (Say et al., 2022). Therefore, our MSC tape with high energy and power density holds promising prospect to advance the practical application in wearable electronics. Additionally, the cycling stability of the MSC-150 was evaluated at a current density of 1 mA cm^{-2} for 4,000 cycles, and nearly 100% of its initial capacitance was retained (Figure 5D).

Electrochemical impedance spectroscopy (EIS) was conducted from 100 kHz to 0.01 Hz to investigate the electrochemical interface properties of MSC-150. The intercept point on the real axis at high frequency in the Nyquist plot (Figure 5E) gives the equivalent series resistance (ESR) of the MSC (Hu et al., 2017). Our MSC-150 possessed a small ESR of about 122 Ω, which is comparable or better than the previously reported work, such as reduced graphene oxide (174 Ω) (Wu et al., 2020), and PEDOT:PSS/MoO_3 (832.2 Ω) (Yoonessi et al., 2019). The device with thickened electrodes showed a smaller ESR, however, the MSC-200 had lower slope in the low frequency region compared with MSC-150 (Supplementary Figure S4), suggesting larger mass transfer resistance, which is consistent with CV results in Figure 4. The absence of a semicircle in the high frequency range indicated the fast ion diffusion in the electrodes (Qi et al., 2019). The nearly vertical line in the low frequency area reflected the capacitive behavior. It can be observed that in the low frequency region of the Bode plot (Figure 5F), the phase angle (−85°) was closer to the value of an ideal capacitor (−90°), revealing the ideal capacitive performance of our MSC. The relaxation time constant, which represents the minimum time required to discharge the energy from the device with an efficiency of more than 50%, can be obtained from the Bode plot with the characteristic frequency (f_0) at the phase angle of −45° where the resistive and capacitive impedances are equal by using the equation $\tau_0 = 1/f_0$ (Qi et al., 2022). The relaxation time constant of the MSC-150 was calculated to be 2.2 s, which is comparable to that of DMSO doped PEDOT:PSS based supercapacitor (2.5 s) (Manjakkal et al., 2020).

The MSC tape could endure severe bending from 0° to 180° (Figure 6A), demonstrating the superior integration capability for wearable electronics. Additional CV tests were conducted to evaluate the electrochemical performance of the MSC under different bending deformations. As shown in Figure 6B, no noticeable distortions in CV curves can be observed when the MSC was bent from flat state to 180°, suggesting the high mechanical stability. Under extreme bending of 180°, the MSC showed a negligible decay in capacitance (Figure 6C). The MSC was then bent from 0° to 180° for 500 cycles, and the areal specific capacitance was remained at 96.2% (Figure 6D). These results confirm the superb durability of our MSC upon mechanical deformations, which is originated from the flexible medical tape substrate, as well as the gel electrolyte layer which serves as the protecting layer to help the PEDOT:PSS electrode maintain its structure (Chen et al., 2014).

Higher voltage or capacitance may be needed to meet the requirements for a specific application. MSC are generally connected in series to boost the operation voltage. Figure 7A shows the picture of three MSC devices connected in series. The

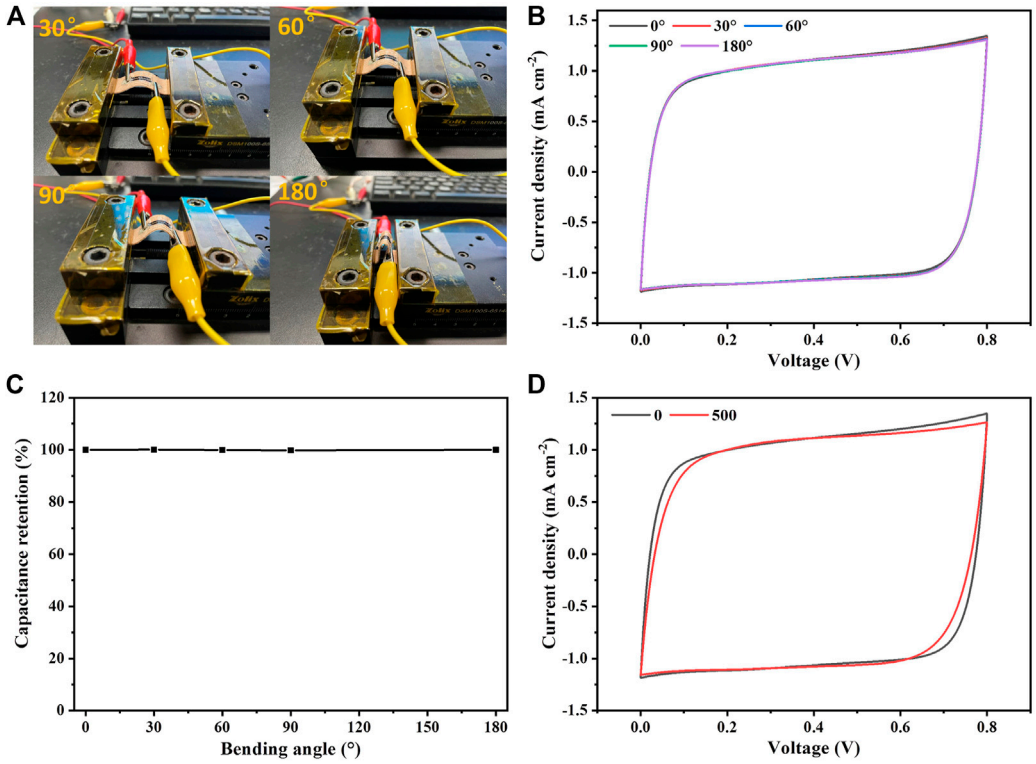

FIGURE 6
(A) Photos of the MSC-150 under bending deformations. **(B)** CV curves (100 mV s^{-1}) and **(C)** capacitance retentions of the MSC-150 under different bending angles. **(D)** CV curves (100 mV s^{-1}) of the MSC-150 after 500 bending cycles.

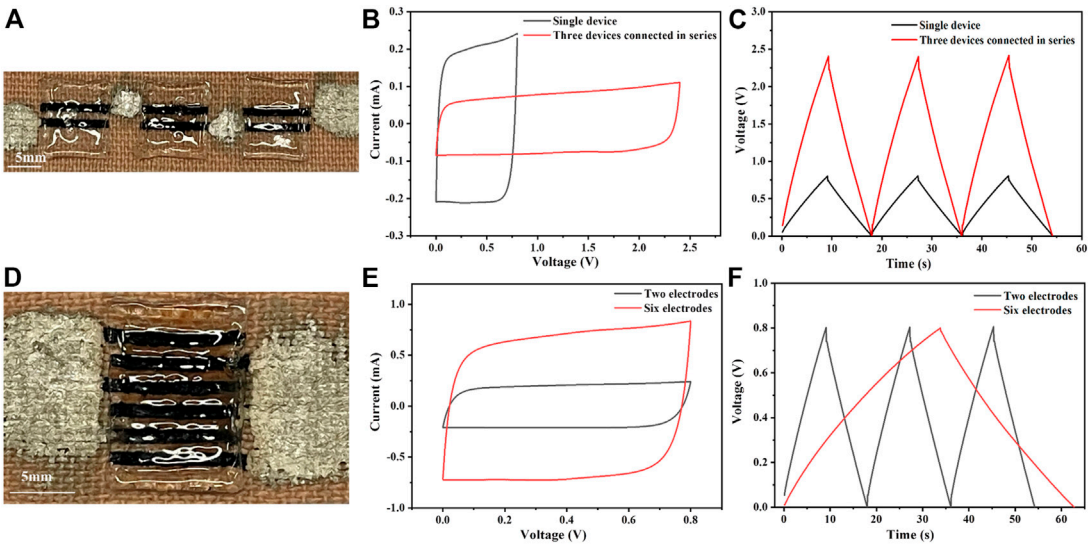

FIGURE 7
(A) Photo of three MSCs connected in series. **(B)** CV curves (100 mV s^{-1}) of a single MSC and three MSCs connected in series. **(C)** GCD curves of a single MSC and three MSCs connected in series at the current of 0.2 mA. **(D)** Photo of a MSC with 6 planar electrodes. **(E)** CV curves (100 mV s^{-1}) of the MSCs with 2 and 6 planar electrodes. **(F)** GCD curves of the MSCs with 2 and 6 electrodes at the current of 0.2 mA.

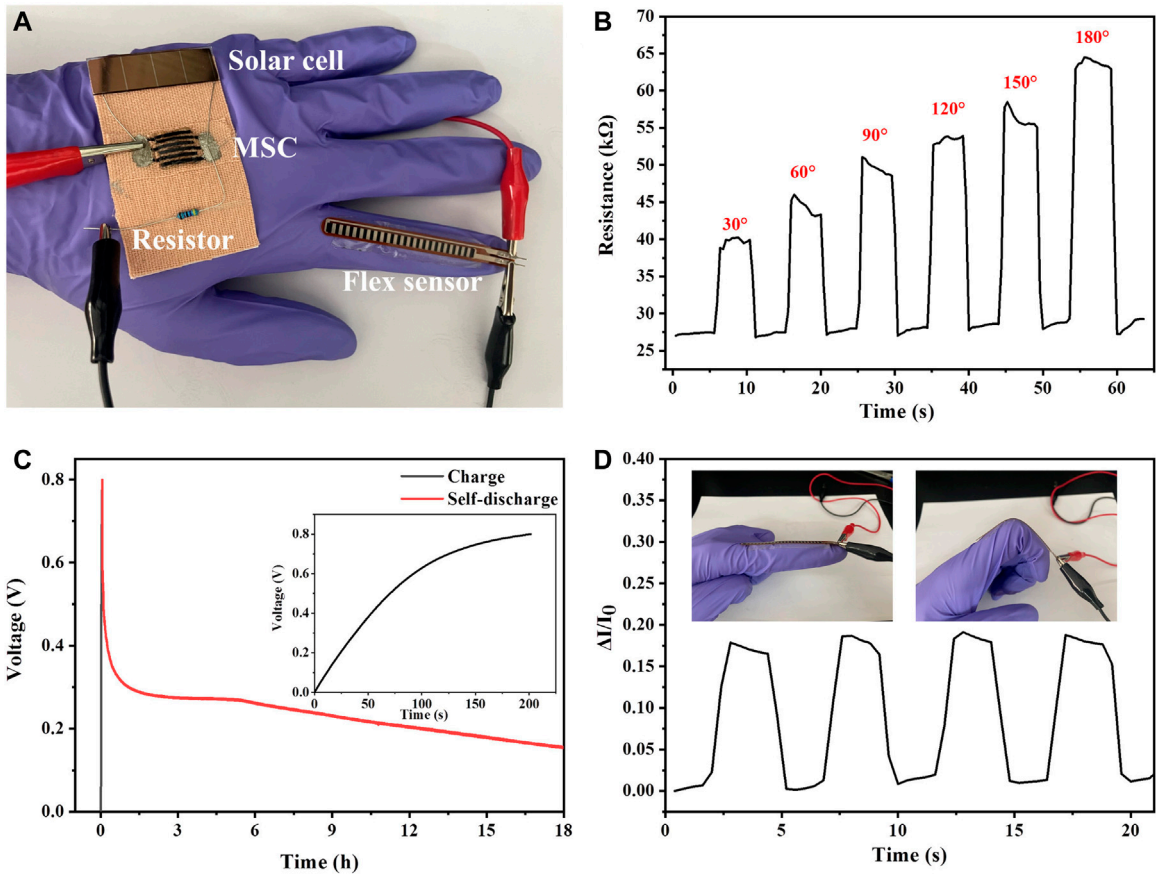

FIGURE 8
(A) Photo of the integrated sensing system. **(B)** Resistance changes of the flex sensor under different bending angles. **(C)** Charging (by the solar cell) and self-discharging curves of the MSC. The inset shows the enlarged charging curve. **(D)** Sensing responses for finger movements. The insets show the bending states of the finger.

CV curves of a single MSC and three MSCs connected in series at the scan rate of 100 mV s^{-1} are presented in Figure 7B. Three MSCs connected in series can effectively increase the voltage to 2.4 V, three times that for a single MSC. In the GCD curves (Figure 7C), three MSCs connected in series tripled the voltage window while retaining nearly the same charging/discharging time. The calculated capacitance of three MSCs connected in series was 0.74 mF, which was about one-third of that of a single MSC (2.27 mF). The capacitance of the MSC can be enhanced simply by employing more pairs of parallel electrodes. Figure 7D shows the picture of a single MSC with three pairs of electrodes. In the CV curves (Figure 7E), the output current of the MSC with 6 electrodes increased by a factor of ~3 compared to that of the MSC with 2 electrodes. Moreover, the charging/discharging time increased by ~3 folds as well compared to that of the MSC with 2 electrodes (Figure 7F). The capacitances of the MSC with 6 and 2 electrodes were 7.27 and 2.27 mF, respectively. These results reflect the feasibility of using our MSC as the basic unit for various output requirements.

Due to the stickiness of the medical tape, the MSC can be conveniently adhered on various substrates to exert its function. For example, the MSC was adhered to the glove, cloth, paper, and wall as shown in Supplementary Figure S5, showing great potential as energy storage devices for wearable electronics and Internet of Things. To explore the practicability of our approach in wearable electronics, the MSC with 6 electrodes was coupled with commercialized solar cell and flex sensor to fabricate an integrated self-powered sensing system (Figure 8A). The MSC could be charged by the solar cell, and then acted as a power source to drive the flex sensor for monitoring the finger movements. The solar cell can work in the indoor environments, which enables various indoor applications. Under the illumination of the indoor LED light, the solar cell showed a short-circuit current of 56 μA and an open-circuit voltage of 2 V (Supplementary Figure S6). The flex sensor is a variable resistor which is sensitive to bending. Its resistance increased with the enlarged bending angles as shown in Figure 8B. The MSC could be charged by the solar cell to 0.8 V in around 200 s, and provided an open-circuit voltage of higher than 0.15 V for 18 h (Figure 8C). Even at the voltage of 0.15 V, the MSC can still power the flex sensor to detect the finger movements. When the finger was bent repeatedly, an obvious

current waveform with about 18% variation of the initial current was recorded (Figure 8D). These results proved that the MSC could work with a solar cell to achieve a stand-alone power supply system for wearable electronics, Internet of Things, and so forth.

4 Conclusion

In summary, we have developed current-collector-free MSC tapes for self-powered strain sensing system. The MSC tapes were fabricated on medical tape by a facile and cost-effective mask-assisted drop-casting method, which can be applied to other aqueous inks. The resulting MSC achieved a high areal capacitance (10.96 mF cm^{-2}) and excellent flexibility (capacitance retention of 96.2% after 500 bending cycles). The MSC can be conveniently attached on various substrates such as glove, cloth, paper and wall due to the stickiness of the medical tape, enabling the application in wearable electronics and Internet of Things. The MSC can be integrated with a solar cell and a flex sensor to build a self-powered strain sensing system, realizing the real-time detection of finger movements. This study provides a strategy for developing adhesive energy storage devices for wearable electronics.

Data availability statement

The original contributions presented in the study are included in the article/Supplementary Material, further inquiries can be directed to the corresponding authors.

Author contributions

Conceptualization, CZ, XZ, and KS; Data curation, WY and CZ; Funding acquisition, CZ, YM, and KS; Investigation, WY; Supervision, CZ; Visualization, WY; Writing–original draft, WY and CZ; Writing–review and editing, CZ, XZ, and KS.

Funding

Financial supports from the Program for Guangdong Introducing Innovative and Entrepreneurial Teams (2016ZT06C412), National Key R&D Program of China (2020YFB0408100), Key-Area Research and Development Program of Guangdong Province (2020B010182001), and the National Natural Science Foundation of China (22105120) are gratefully acknowledged.

Conflict of interest

The authors declare that the research was conducted in the absence of any commercial or financial relationships that could be construed as a potential conflict of interest.

Publisher's note

All claims expressed in this article are solely those of the authors and do not necessarily represent those of their affiliated organizations, or those of the publisher, the editors and the reviewers. Any product that may be evaluated in this article, or claim that may be made by its manufacturer, is not guaranteed or endorsed by the publisher.

Supplementary material

The Supplementary Material for this article can be found online at: https://www.frontiersin.org/articles/10.3389/fmats.2023.1162270/full#supplementary-material

References

An, T., Ling, Y., Gong, S., Zhu, B., Zhao, Y., Dong, D., et al. (2019). A wearable second skin-like multifunctional supercapacitor with vertical gold nanowires and electrochromic polyaniline. *Adv. Mat. Technol.* 4 (3), 1800473. doi:10.1002/admt.201800473

Chen, T., Xue, Y., Roy, A. K., and Dai, L. (2014). Transparent and stretchable high-performance supercapacitors based on wrinkled graphene electrodes. *ACS Nano* 8 (1), 1039–1046. doi:10.1021/nn405939w

Chen, Y.-T., Ma, C.-W., Chang, C.-M., and Yang, Y.-J. (2018). Micromachined planar supercapacitor with interdigital buckypaper electrodes. *Micromachines* 9 (5), 242. doi:10.3390/mi9050242

Gao, C., Gao, J., Shao, C., Xiao, Y., Zhao, Y., and Qu, L. (2018). Versatile origami micro-supercapacitors array as a wind energy harvester. *J. Mat. Chem. A* 6 (40), 19750–19756. doi:10.1039/C8TA05148H

Hu, H., Pei, Z., Fan, H., and Ye, C. (2016). 3D interdigital Au/MnO_2/Au stacked hybrid electrodes for on-chip microsupercapacitors. *Small* 12 (22), 3059–3069. doi:10.1002/smll.201503527

Hu, M., Li, Z., Li, G., Hu, T., Zhang, C., and Wang, X. (2017). All-solid-state flexible fiber-based MXene supercapacitors. *Adv. Mat. Technol.* 2 (10), 1700143. doi:10.1002/admt.201700143

Kim, D., Lee, G., Kim, D., and Ha, J. S. (2015). Air-stable, high-performance, flexible microsupercapacitor with patterned ionogel electrolyte. *ACS Appl. Mat. Interfaces* 7 (8), 4608–4615. doi:10.1021/am5077843

Kurra, N., Ahmed, B., Gogotsi, Y., and Alshareef, H. N. (2016). MXene-on-paper coplanar microsupercapacitors. *Adv. Energy Mat.* 6 (24), 1601372. doi:10.1002/aenm.201601372

Lin, Y., Chen, J., Tavakoli, M. M., Gao, Y., Zhu, Y., Zhang, D., et al. (2019). Printable fabrication of a fully integrated and self-powered sensor system on plastic substrates. *Adv. Mat.* 31 (5), 1804285. doi:10.1002/adma.201804285

Liu, S., Xie, J., Li, H., Wang, Y., Yang, H. Y., Zhu, T., et al. (2014). Nitrogen-doped reduced graphene oxide for high-performance flexible all-solid-state micro-supercapacitors. *J. Mat. Chem. A* 2 (42), 18125–18131. doi:10.1039/C4TA03192J

Liu, W.-W., Feng, Y.-Q., Yan, X.-B., Chen, J.-T., and Xue, Q.-J. (2013). Superior micro-supercapacitors based on graphene quantum dots. *Adv. Funct. Mat.* 23 (33), 4111–4122. doi:10.1002/adfm.201203771

Liu, Y., Weng, B., Xu, Q., Hou, Y., Zhao, C., Beirne, S., et al. (2016). Facile fabrication of flexible microsupercapacitor with high energy density. *Adv. Mat. Technol.* 1 (9), 1600166. doi:10.1002/admt.201600166

Manjakkal, L., Pullanchiyodan, A., Yogeswaran, N., Hosseini, E. S., and Dahiya, R. (2020). A wearable supercapacitor based on conductive PEDOT:PSS-coated cloth and a sweat electrolyte. *Adv. Mat.* 32 (24), 1907254. doi:10.1002/adma.201907254

Ouyang, J., Xu, Q., Chu, C.-W., Yang, Y., Li, G., and Shinar, J. (2004). On the mechanism of conductivity enhancement in poly(3,4-ethylenedioxythiophene): poly(styrene sulfonate) film through solvent treatment. *Polymer* 45 (25), 8443–8450. doi:10.1016/j.polymer.2004.10.001

Pu, X., Liu, M., Li, L., Han, S., Li, X., Jiang, C., et al. (2016). Wearable textile-based in-plane microsupercapacitors. *Adv. Energy Mat.* 6 (24), 1601254. doi:10.1002/aenm.201601254

Qi, F., Tang, Y., Zhao, C., Zheng, Z., Jia, X., and Min, Y. (2022). Device-scaled controlled crumpling of MXene-based ultrathin supercapacitors as stretchable power sources. *ACS Appl. Energy Mat.* 5 (4), 4296–4306. doi:10.1021/acsaem.1c03892

Qi, F., Zhao, C., Wang, C., Jia, X., Weng, L., He, T., et al. (2019). Polyaniline electrochemically deposited on tailored metal mesh for dynamically stretchable supercapacitors. *J. Electrochem. Soc.* 166 (16), A3932–A3939. doi:10.1149/2.0011916jes

Salles, P., Quain, E., Kurra, N., Sarycheva, A., and Gogotsi, Y. (2018). Automated scalpel patterning of solution processed thin films for fabrication of transparent MXene microsupercapacitors. *Small* 14 (44), 1802864. doi:10.1002/smll.201802864

Say, M. G., Sahalianov, I., Brooke, R., Migliaccio, L., Głowacki, E. D., Berggren, M., et al. (2022). Ultrathin paper microsupercapacitors for electronic skin applications. *Adv. Mat. Technol.* 7 (8), 2101420. doi:10.1002/admt.202101420

Shao, Y., Li, J., Li, Y., Wang, H., Zhang, Q., and Kaner, R. B. (2017). Flexible quasi-solid-state planar micro-supercapacitor based on cellular graphene films. *Mat. Horiz.* 4 (6), 1145–1150. doi:10.1039/C7MH00441A

Tian, W., VahidMohammadi, A., Reid, M. S., Wang, Z., Ouyang, L., Erlandsson, J., et al. (2019). Multifunctional nanocomposites with high strength and capacitance using 2D MXene and 1D nanocellulose. *Adv. Mat.* 31 (41), 1902977. doi:10.1002/adma.201902977

Wang, K., Zou, W., Quan, B., Yu, A., Wu, H., Jiang, P., et al. (2011). An all-solid-state flexible micro-supercapacitor on a chip. *Adv. Energy Mat.* 1 (6), 1068–1072. doi:10.1002/aenm.201100488

Wang, Y., Shi, Y., Zhao, C. X., Wong, J. I., Sun, X. W., and Yang, H. Y. (2014). Printed all-solid flexible microsupercapacitors: Towards the general route for high energy storage devices. *Nanotechnology* 25 (9), 094010. doi:10.1088/0957-4484/25/9/094010

Wu, Y., Zhang, Y., Liu, Y., Cui, P., Chen, S., Zhang, Z., et al. (2020). Boosting the electrochemical performance of graphene-based on-chip micro-supercapacitors by regulating the functional groups. *ACS Appl. Mat. Interfaces* 12 (38), 42933–42941. doi:10.1021/acsami.0c11085

Wu, Z.-S., Parvez, K., Li, S., Yang, S., Liu, Z., Liu, S., et al. (2015). Alternating stacked graphene-conducting polymer compact films with ultrahigh areal and volumetric capacitances for high-energy micro-supercapacitors. *Adv. Mat.* 27 (27), 4054–4061. doi:10.1002/adma.201501643

Xue, M., Xie, Z., Zhang, L., Ma, X., Wu, X., Guo, Y., et al. (2011). Microfluidic etching for fabrication of flexible and all-solid-state micro supercapacitor based on MnO_2 nanoparticles. *Nanoscale* 3 (7), 2703–2708. doi:10.1039/C0NR00990C

Yang, J., Hong, T., Deng, J., Wang, Y., Lei, F., Zhang, J., et al. (2019). Stretchable, transparent and imperceptible supercapacitors based on Au@MnO_2 nanomesh electrodes. *Chem. Commun.* 55 (91), 13737–13740. doi:10.1039/C9CC06263G

Yoonessi, M., Borenstein, A., El-Kady, M. F., Turner, C. L., Wang, H., Stieg, A. Z., et al. (2019). Hybrid transparent PEDOT:PSS molybdenum oxide battery-like supercapacitors. *ACS Appl. Energy Mat.* 2 (7), 4629–4639. doi:10.1021/acsaem.8b02258

Yun, J., Kim, D., Lee, G., and Ha, J. S. (2014). All-solid-state flexible micro-supercapacitor arrays with patterned graphene/MWNT electrodes. *Carbon* 79, 156–164. doi:10.1016/j.carbon.2014.07.055

Zhang, C., Peng, Z., Huang, C., Zhang, B., Xing, C., Chen, H., et al. (2021). High-energy all-in-one stretchable micro-supercapacitor arrays based on 3D laser-induced graphene foams decorated with mesoporous ZnP nanosheets for self-powered stretchable systems. *Nano Energy* 81, 105609. doi:10.1016/j.nanoen.2020.105609

Zhao, C., Jia, X., Shu, K., Yu, C., Wallace, G. G., and Wang, C. (2020). Conducting polymer composites for unconventional solid-state supercapacitors. *J. Mat. Chem. A* 8 (9), 4677–4699. doi:10.1039/C9TA13432H

Zhao, C., Liu, Y., Beirne, S., Razal, J., and Chen, J. (2018). Recent development of fabricating flexible micro-supercapacitors for wearable devices. *Adv. Mat. Technol.* 3 (9), 1800028. doi:10.1002/admt.201800028

Zhao, C., Wang, C., Yue, Z., Shu, K., and Wallace, G. G. (2013). Intrinsically stretchable supercapacitors composed of polypyrrole electrodes and highly stretchable gel electrolyte. *ACS Appl. Mat. Interfaces* 5 (18), 9008–9014. doi:10.1021/am402130j

Zheng, S., Shi, X., Das, P., Wu, Z.-S., and Bao, X. (2019). The road towards planar microbatteries and micro-supercapacitors: From 2D to 3D device geometries. *Adv. Mat.* 31 (50), 1900583. doi:10.1002/adma.201900583

Zhu, M., Huang, Y., Huang, Y., Li, H., Wang, Z., Pei, Z., et al. (2017). A highly durable, transferable, and substrate-versatile high-performance all-polymer micro-supercapacitor with plug-and-play function. *Adv. Mat.* 29 (16), 1605137. doi:10.1002/adma.201605137

Zhu, S., Li, Y., Zhu, H., Ni, J., and Li, Y. (2019). Pencil-drawing skin-mountable micro-supercapacitors. *Small* 15 (3), 1804037. doi:10.1002/smll.201804037